

Aperiodic Bragg Reflectors for Tunable High-Purity Structural Color Based on Phase Change Material

Sambhu Jana,^{II} Kandammathe Valiyaveedu Sreekanth,^{II} Omar A. M. Abdelraouf, Ronghui Lin, Hong Liu, Jinghua Teng,^{*} and Ranjan Singh^{*}



Cite This: *Nano Lett.* 2024, 24, 3922–3929



Read Online

ACCESS |

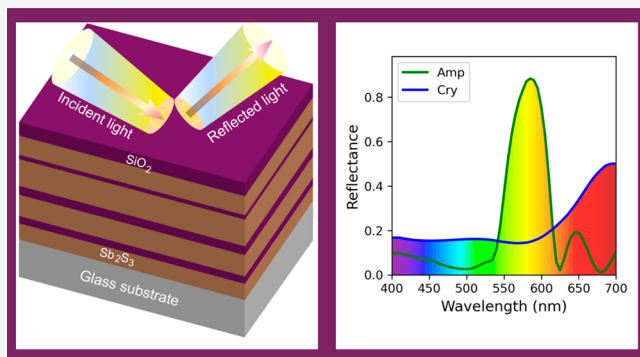
Metrics & More

Article Recommendations

Supporting Information

ABSTRACT: Tunable thin-film coating-based reflective color displays have versatile applications including image sensors, camouflage devices, spatial light modulators, and intelligent windows. However, generating high-purity colors using such coatings have posed a challenge. Here, we reveal high-purity color generation using an ultralow-loss phase change material (Sb_2S_3)-based tunable aperiodic distributed Bragg reflector (A-DBR). By strategically adjusting the periodicity of the adjacent layers of A-DBRs, we realize a narrow photonic bandgap with high reflectivity to generate high-purity orange and yellow colors. In particular, we demonstrate an A-DBR with a large photonic bandgap tunability by changing the structural phase of Sb_2S_3 layers from amorphous to crystalline. Moreover, we experimentally tailor multistate tunable colors through external optical stimuli. Unlike conventional nano thin-film coatings, our proposed approach offers an irradiance-free, narrowband, and highly reflective color band, achieving exceptional color purity by effectively suppressing reflections in off-color bands.

KEYWORDS: thin-film coatings, color filters, phase change materials, aperiodic distributed Bragg reflectors



Conventional color filters composed of pigments and synthetic dyes rely on chemical compositions for the selective absorption of light from different colors.¹ The main issues associated with these color filters are (i) degradation in the filtering performances due to their relatively limited chemical stability and (ii) the necessity of integrating numerous pigments or dyes to realize a complete Bayer color scheme, which is very expensive and challenging. Researchers addressed these issues by modifying the surface structure of solid materials, which enables the manipulation of light–matter interactions through scattering, reflection, absorption, transmission, or a combination thereof, resulting in the generation of visible colors. This revolutionary breakthrough spurred the rapid growth of various structural coloring techniques, which include surface plasmon resonances,² nanowire waveguides,³ metamaterials,^{4,5} quantum dots,^{6,7} and nanogratings.⁸ These structural coloring approaches have received extensive attention because of their several advantages over traditional color filters such as environmental friendliness, high efficiency, broad spectrum tunability, exceptional color stability, and robustness from chemical degradation caused by ultraviolet exposure and heat. As a result, the generation and tuning of versatile nanostructural colors have a plethora of applications, including displays,⁹ anticounterfeiting systems, solar cells,¹⁰ colorimetric sensors,^{11,12} and decorative objects.¹

However, most of these structural coloring platforms limit their practical applications on a large scale by various factors such as incident angle and polarization sensitivity, off-resonant wavelength components, and high-precision nanofabrication processes.

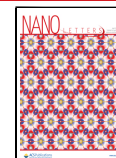
In recent years, thin-film optical coatings have gained a lot of interest and have extensively resolved the issues associated with nanostructural color filters, primarily because of their large scalability, cost-effectiveness, and facile lithography-free nanofabrication.¹³ In general, typical thin-film coatings are composed of metal–dielectric–metal (MDM) cavities and produce colors through selective absorption of light.^{14,15} Nevertheless, the main drawbacks associated with these MDM thin film coatings are of poor color purity and generate iridescent and distinct colors in the reflection and transmission modes. Lately, ElKabbash et al. adeptly tackled these issues by introducing a novel type of thin-film coating consisting of a broadband and a narrowband absorber, which produces colors

Received: January 4, 2024

Revised: March 13, 2024

Accepted: March 15, 2024

Published: March 20, 2024



ACS Publications

© 2024 American Chemical Society

3922

<https://doi.org/10.1021/acs.nanolett.4c00052>
Nano Lett. 2024, 24, 3922–3929

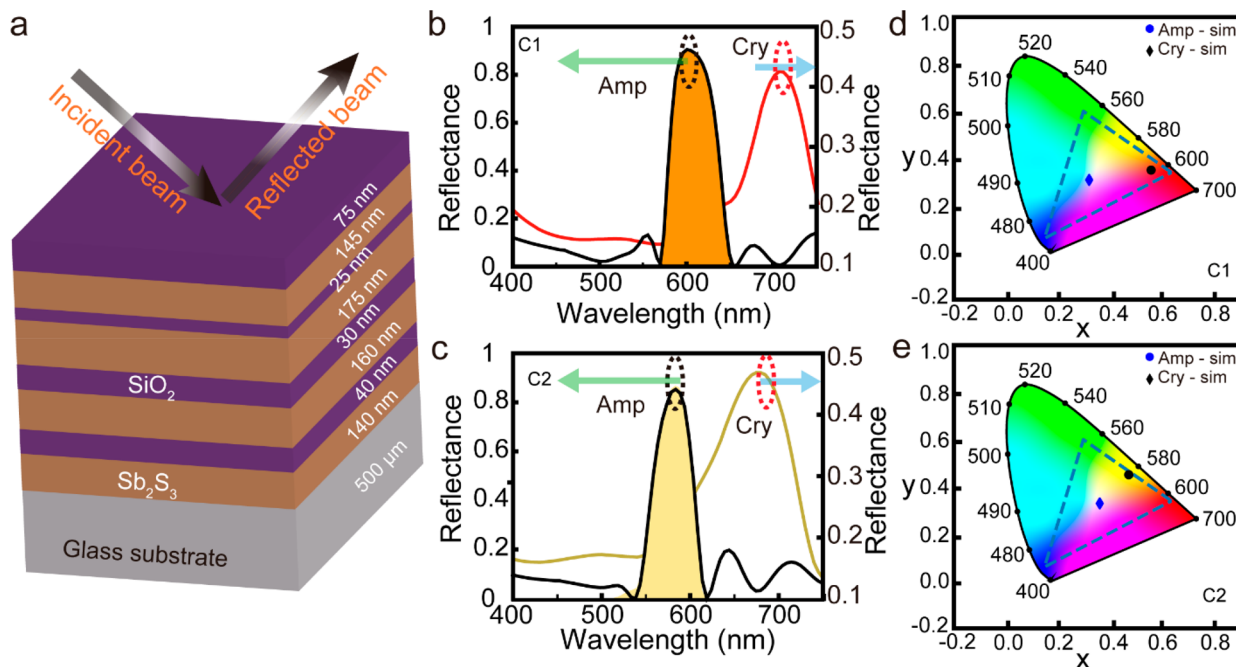


Figure 1. (a) Schematic structure of an A-DBR (C1) comprised of alternating layers of Sb₂S₃ and SiO₂ with different thicknesses. Numerically calculated reflectance spectra at normal incidence for (b) orange and (c) yellow bands, considering both the amorphous (amp) and crystalline (cry) phases of Sb₂S₃ layers. The green and cyan arrows represent the reflectance axis corresponding to the amorphous and crystalline phases of Sb₂S₃. CIE 1931 chromaticity diagram displaying the colors associated with the calculated reflection spectrum for the structural configurations (d) C1 and (e) C2 with both phases (amp and cry) of Sb₂S₃.

due to the generation of the asymmetric Fano resonance.^{16–18} In a brief span, this color scheme has gained significant attention among researchers because of its numerous distinctive attributes, such as the ability to produce the same iridescent-free colors in both reflection and transmission modes, along with high resolution and purity.^{19,20} Recently, dynamically tunable structural coloring was demonstrated by incorporating nonvolatile phase change materials (PCMs) into FROC,^{21–25} as PCMs have received great attention due to their rapid switching speed, stable memory beyond the transition temperature, large refractive index contrast, and tunable optical responses across a wide range of wavelengths from ultraviolet to terahertz.^{5,26–30} Although this discovery would bring many opportunities in the field of nanophotonics^{31–33} including structural coloring, there are certain drawbacks associated with reflective tunable FROC-based color filters that require further research. The main shortcomings are (i) a broad and asymmetric Fano resonance spectrum hinders achieving a selective narrow reflection band in the visible spectrum, (ii) the presence of off-resonance reflections impacts the color purity, and (iii) absorption loss due to metal and lossy dielectric material hinders the attainment of highly reflective Fano resonance with narrow line width.

Here, we experimentally demonstrate PCM-based tunable aperiodic distributed Bragg reflectors (A-DBRs) for high-purity structural coloring. The proposed tunable A-DBRs are made up of alternating layers of SiO₂ and ultralow-loss PCM such as Sb₂S₃, with a total thickness of < 800 nm. Importantly, we demonstrate multistate forward tunable colors by switching the phase of Sb₂S₃ layers with laser-induced heating. As an advantage, the proposed coating provides a substantially high-purity color band by suppressing the off-band reflections, and it is independent of the incident angle and polarization. We also

propose a machine-learning approach to realize high-purity colors in both amorphous and crystalline phases of A-DBR. In contrast to conventional tunable MDM cavities and newly developed FROC coatings, the proposed nano thin-film coatings exhibit substantially high and narrowband selective reflection in the visible spectral band.

■ DESIGN OF A-DBR-BASED HIGH-PURITY REFLECTIVE COLORS

DBR is a superlattice structure of thin film coatings comprising alternating materials with high and low refractive indices.³⁴ The high reflectivity obtained in DBRs is due to the constructive interference of light reflecting across multiple interfaces, which is given by the following equation:³⁵

$$R_{\max} = \left[\frac{1 - \left(\frac{n_s}{n_0} \right) \left(\frac{n_1}{n_2} \right)^{2N}}{1 + \left(\frac{n_s}{n_0} \right) \left(\frac{n_1}{n_2} \right)^{2N}} \right]^2 \quad (1)$$

where N is the number of periods in the structure and n_s, n₀, n₁, and n₂ are the refractive indices of the substrate, surrounding medium (air), and the high- and low-index materials, respectively. Thus, by increasing both the number of periods and the refractive index contrast ($\Delta n = n_1 - n_2$) between them, a broad and highly reflective Bragg reflection can be attained. In general, conventional DBRs are composed of any combinations of transparent materials exhibiting a high-index contrast, which may include metal-oxides, organic polymers, semiconductors, or combinations thereof.³⁶ In contrast to these materials, PCMs possess an exceptionally high refractive index, thereby minimizing the required number of layers within the structure to attain an equivalent level of reflectance. However, PCM-based DBR structures and their potential

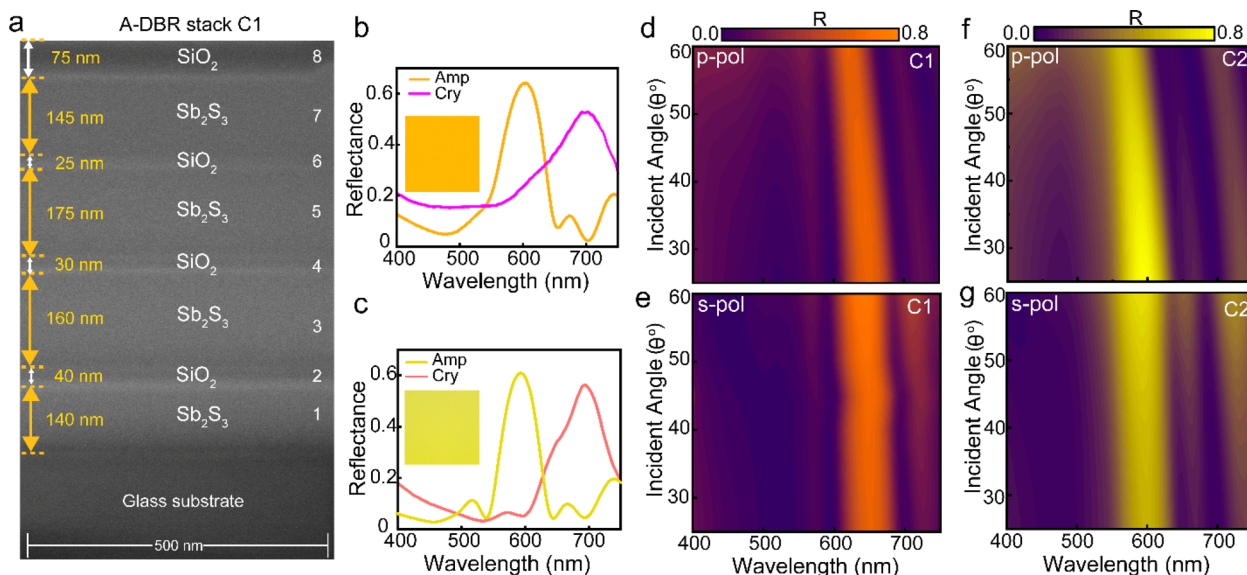


Figure 2. Experimentally measured angle-resolved reflection spectra of the A-DBR. (a) Scanning electron microscopic image of the fabricated orange sample (C1) is presented in the amorphous state, and the corresponding alternate layers of Sb_2S_3 and SiO_2 are designated by nos. 1–8. Reflectance spectra at normal incidence for both amp and cry phases of Sb_2S_3 of configurations (b) C1 and (c) C2. The insets represent the high-resolution optical microscopic images of the fabricated samples corresponding to two different colors with amorphous Sb_2S_3 . Measured 2D map of angular reflection spectra of the amp A-DBR configuration C1 for (d) p-polarization and (e) s-polarization. Measured 2D map of angular reflection spectra of amp A-DBR configuration C2 for (f) p-polarization and (g) s-polarization.

application as a color filter remain limited due to their inherent absorption within the visible spectral region despite numerous novel functionalities^{37–39} and high refractive index. In order to realize an actively tunable DBR for high-purity color generation, we select an ultralow loss PCM such as Sb_2S_3 to serve as the high refractive index layers in the DBR. Note that Sb_2S_3 exhibits a high refractive index with ultralow-loss response at wavelengths > 560 nm in the amorphous phase. Transfer-matrix method (TMM) was employed to compute the expected reflectance spectra, involving the fitting of the complex refractive index of Sb_2S_3 measured through ellipsometry within the visible range (see Supporting Information Figure S1). Figure 1a shows a pictorial diagram of the proposed PCM incorporated A-DBR with alternating layers of Sb_2S_3 and SiO_2 stacked on a glass substrate. Sb_2S_3 provides a refractive index contrast (Δn) of ~ 1.76 at 590 nm wavelength by combining with the SiO_2 layer. Due to the high refractive index contrast, DBR generates a highly reflective spectrum even with a minimal number of 4 bilayers.

To achieve a narrowband and highly reflective Bragg spectrum that fully encompasses a specific color band, we strategically modified the thickness of individual layers within the DBR. We designed two A-DBR structures to realize orange and yellow colors, which consisted of 4 bilayers of Sb_2S_3 – SiO_2 (Figure 1a). The structural arrangement of the A-DBR designed for the orange (C1) color stack is illustrated in Figure 1, with the corresponding thicknesses of the layers from bottom to top highlighted in the figure. In contrast, the thicknesses of the yellow (C2) color stack, from bottom to top, are 130, 50, 145, 35, 160, 18, 145, and 70 nm. It is important to note that the thickness of alternate layers is not uniform, but the total thickness of each bilayer increases gradually from the bottom (substrate side) to the top. As shown in Figure 1b,c, the central wavelengths of the highly reflective ($\sim 90\%$) photonic bandgap (PBG) for the C1 and C2 configurations with amorphous Sb_2S_3 are 605 and 585 nm, respectively,

representing the orange and yellow color bands. Notably, a significant PBG tunability of ~ 110 nm is obtained by changing the structural phase of Sb_2S_3 layers from amorphous to crystalline, as shown by the red and pear color lines in Figure 1b,c. Conversely, a periodic DBR consisting of amp- Sb_2S_3 produces a very broad PBG in the visible region (see Supporting Information Figure S2).

To facilitate visualization of the color response of the filters concerning the amorphous phase of Sb_2S_3 , the chromaticity coordinates derived from numerically calculated reflectance spectra for C1 and C2 are depicted in Figure 1d,e, respectively. Figure 1d illustrates the chromaticity coordinates for the C1 stack, while Figure 1e represents the same for stack C2. Furthermore, color mixing is a regular problem in structural color filters, mainly due to the presence of off-resonant components and broad resonance peaks. However, color purity refers to the degree of purity of colors that is free from mixing white light or other colors. This can be computed by using the following equation:^{40–42}

$$\text{color purity} = \frac{\sqrt{(x - x_{\text{std}})^2 + (y - y_{\text{std}})^2}}{\sqrt{(x_c - x_{\text{std}})^2 + (y_c - y_{\text{std}})^2}} \times 100 \quad (2)$$

where x and y are the CIE coordinates of the entire spectrum, x_{std} and y_{std} are the CIE coordinates of the standard illuminates of white light, and x_c and y_c are the CIE coordinates at the central wavelength. The obtained color purity with amp- Sb_2S_3 for the orange and yellow colors are 88% and 82%, respectively, which is remarkable compared with other PCM-based color filters. Note that the color purity of PCM-based FROCs^{21,25,43} is about 35–40%, significantly lower compared to the color purity reported in this study. This disparity arises from the broad Fano-resonance peak and the metallic losses induced by the presence of the lossy PCM (GST) and metal layers.^{17,21} Therefore, the proposed A-DBR based color filter has several advantages over the existing PCM-based FROCs

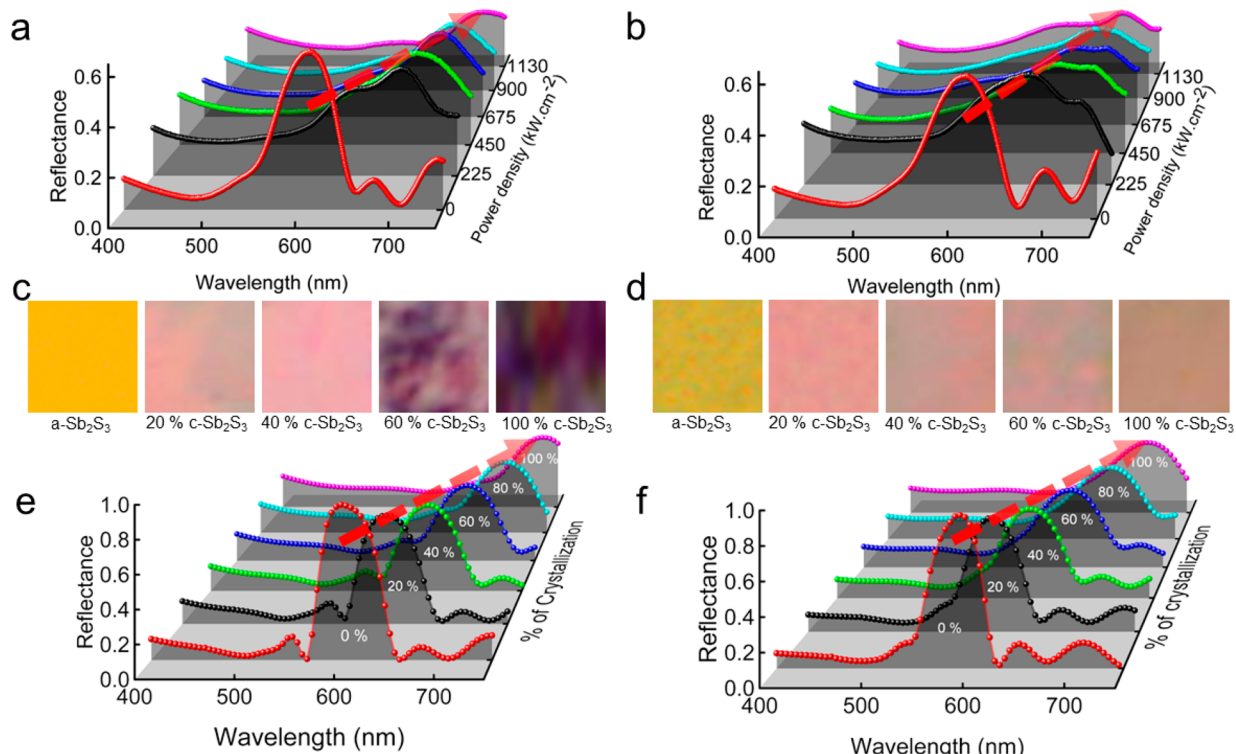


Figure 3. 3D color mapping of the reflectance spectra of A-DBR in different crystalline states of Sb_2S_3 . Measured reflectance spectra for configurations (a) C1 and (b) C2 at different laser power densities. The red dashed arrow denotes the shift in a central wavelength corresponding to varying degrees of crystallinity from 0 to 100%. The optical microscopic image illustrates the achieved color tunability with different levels of crystallinity for (c) the C1 configuration and (d) the C2 configuration. The calculated reflectance spectra of configurations (e) C1 and (f) C2 at different levels of crystallinity.

due to its selective narrowband reflection. In this context, we included a comparison table (Table S1) in the **Supporting Information**, presenting detailed information on the diverse properties of various phase-change materials (PCMs) and their utilization as color filters in FROC and FP cavity-based devices. We further calculated the spectral selectivity to obtain more comprehensive insight about the color purity of the proposed structure.⁴⁴ The calculated spectral selectivity with amp- Sb_2S_3 for the orange and yellow colors are 76% and 67% respectively, which demonstrates remarkable performance compared to other PCM-based color filters.

■ EXPERIMENTAL DEMONSTRATION OF A-DBR-BASED REFLECTIVE COLOR FILTERS

We fabricated the two color configurations using thin-film deposition techniques (**Supporting Information**). The thicknesses of individual layers of the A-DBR were confirmed using an ellipsometer. Figure 2a displays the cross-sectional scanning electron microscopy (SEM) image of the fabricated Sb_2S_3 – SiO_2 A-DBR (for the orange color). For the amorphous (amp) phase of Sb_2S_3 , the measured reflectance spectra of A-DBR at normal incidence for configurations C1 and C2 are represented in Figure 2b,c, respectively. As can be seen, the spectral bands (PBG) of both configurations correlate well with the calculated results, and the measured color purity for configurations C1 and C2 with amp- Sb_2S_3 are 63% and 59%, respectively. The decrease in reflectance amplitude and the consequential decline in color purity can primarily be attributed to the inherent surface roughness of the film, variations in the individual thickness of the fabricated thin films, and limitations in the spectral resolution of the measurement setup. In Figure

2b,c, we also display the reflectance spectrum of C1 and C2 when the Sb_2S_3 layers are in the crystalline (cry) phase, where the samples were annealed at 300 °C to change the phase of Sb_2S_3 from amorphous to crystalline. A significant red shift with central wavelength shifts of 110 and 87 nm is obtained for C1 and C2, respectively, particularly toward the red color spectral band. However, the reflection spectral band slightly broadened and off-band reflection increased due to the inherent losses of cry- Sb_2S_3 . Therefore, the obtained color purity of cry A-DBR is lower compared to amp A-DBR (see Supporting Information Figure S3).

In addition, we investigate the effect of incident angle and polarization on the color purity of the fabricated A-DBR structures, as these factors ensure reliable and stable color reproduction under diverse conditions. For amp A-DBR structures, the measured angular reflection spectra (25–60°) of C1 and C2 configurations for p- and s-polarizations are shown in Figure 2d–e and Figure 2f–g, respectively. The corresponding calculated results are shown in the Supporting Information Figure S4. It is visible that the color bands of both polarizations are almost uniform for an incident angle of up to 60°. However, the color bandwidth slightly diminishes for p-polarized light when the incident angle increases > 60°, which is due to the Brewster effect occurring at the interface between SiO_2 and Sb_2S_3 layers. Conversely, with s-polarized light, the reflective efficiency and the color bandwidth remain the same for both the orange and yellow colors even when the incident angle increases > 60°. Overall, the proposed A-DBR structures exhibit incident angle- and polarization-independent responses for high-purity colors.

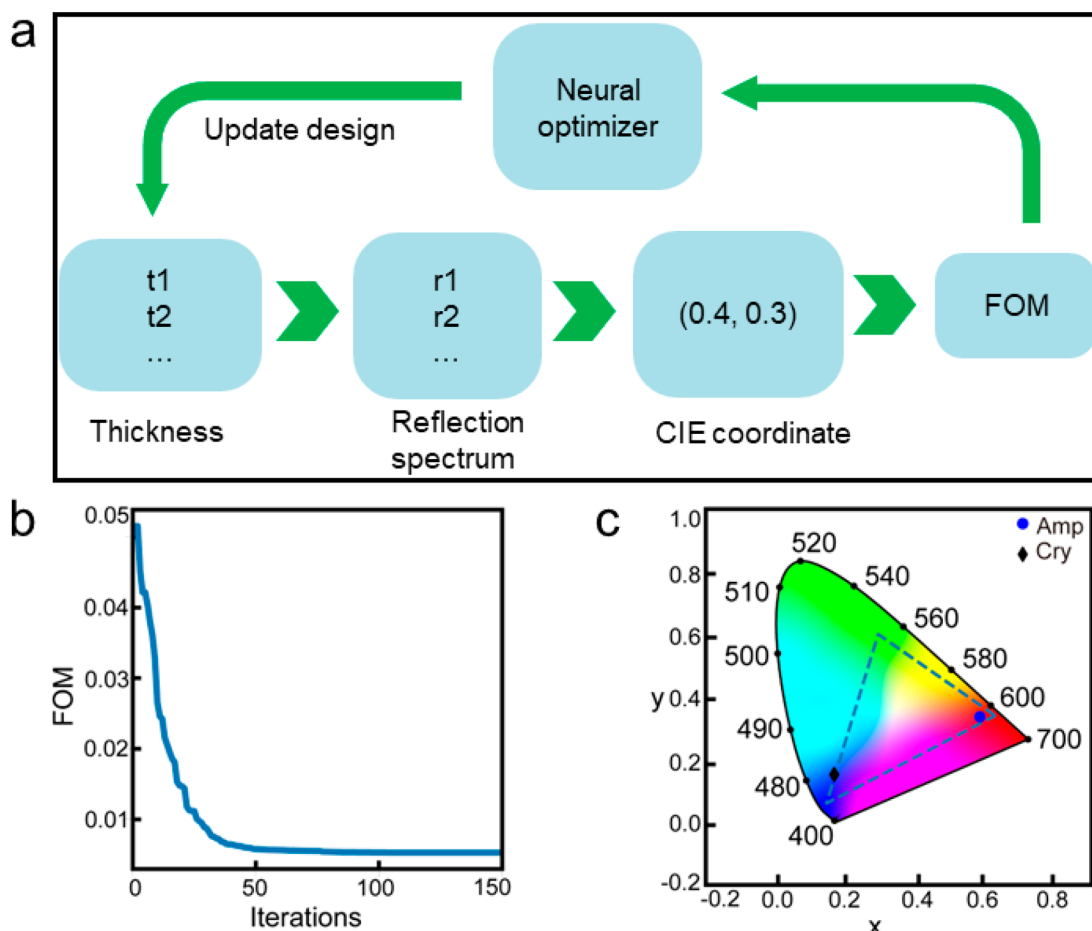


Figure 4. (a) Flowchart of the optimization algorithm. (b) FOM function evolution during the optimization. Optimization of the DBR design maximized the color contrast between amorphous and crystalline DBR. (c) Corresponding color coordinates of the amorphous (pure red) and crystalline (pure blue) DBR.

Since the development of nanophotonic devices demand actively tunable components, we demonstrate optically controlled continuous forward color tuning by directing a high-power continuous-wave (CW) laser onto the sample surface. In the experiment, upon exposing the high-power CW laser on the sample, the structural phase transformation of Sb₂S₃ initiates. By incremental adjustment of the average laser power, an intermediate state with partial crystallinity emerges. We considered that in the intermediate stage, the degree of crystallinity of Sb₂S₃ can be regarded as a mixture of amorphous and crystalline molecules with different proportions. The effective dielectric constant of the partially crystallized Sb₂S₃ can be represented by an effective-medium theory using the Lorentz–Lorenz relation, which is expressed as^{14,45}

$$\frac{\epsilon_{\text{int}} - 1}{\epsilon_{\text{int}} + 2} = p \frac{\epsilon_{\text{cry}} - 1}{\epsilon_{\text{cry}} + 2} + (1 - p) \frac{\epsilon_{\text{amp}} - 1}{\epsilon_{\text{amp}} + 2} \quad (3)$$

where ϵ_{int} , ϵ_{amp} , and ϵ_{cry} are the dielectric constants of Sb₂S₃ in the intermediate, amorphous, and crystalline phases, respectively. The variable “ p ” ranges between 0 (representing amorphous Sb₂S₃) and 1 (indicating crystalline Sb₂S₃), symbolizing the degree of crystallization. Subsequently, we conducted Raman spectroscopy, as depicted in Supporting Information Figure S5, in order to scrutinize changes in the crystallinity of PCM, revealing significant insights. To induce

crystallization, a continuous-wave (CW) laser with a wavelength of 532 nm and an average power of 6 mW was utilized. The Raman spectrum obtained with amp-Sb₂S₃ reveals two broad bands at approximately ~290 and ~100 cm⁻¹, corresponding to the vibrational Sb–Sb bonds in the S₂Sb–SbS₂ structural units and SbS₃ pyramids, respectively.^{46,47} The observed transformation from an amorphous state (as-deposited) to a fully crystalline phase was marked by a discernible shift in Raman peaks, progressing from 90 to 275 cm⁻¹. This shift became apparent as the laser exposure time to the sample increased.

To experimentally demonstrate continuous forward tuning of the structural color band, we employ a photoscanning microscope and a CW laser with a wavelength of 532 nm. By gradually changing the power density of the laser, ranging from 225 to 1,130 kW/cm² while maintaining a constant scanning speed of 20 μm/s and a line step width of 333 nm, we can attain discernible intermediate states. Experimentally measured reflectance spectra for orange and yellow color bands at different levels of crystallinity of Sb₂S₃ with the application of variable laser power density are shown in Figure 3a,b, respectively. For the amorphous A-DBR, the central wavelengths of the measured reflected color bands for C1 and C2 are 605 and 595 nm, respectively. With increasing laser power density, the color bands of both configurations are continuously shifted toward the spectral band of red color. For a very high pump power density (≥ 1130 kW/cm²), the A-

DBR was fully crystallized and no further wavelength shift was observed. The continuous red-shifting and broadening in the color band at the intermediate and crystalline states are attributed to the high crystallinity that shrinks the film thickness and increases the inherent optical losses in the Sb₂S₃ layers. Also note that upon reaching 100% crystallinity, the amplitude contrast of the Bragg reflected color band diminishes significantly due to intense absorption losses and the attainment of a high refractive index, resulting in broader spectra. The optical microscopic images displayed in Figure 3c,d, respectively, show that both structures gradually change their initial color (for amp-Sb₂S₃) toward red by controlling the laser power delivered to the DBR during the crystallization process. These findings emphasize the flexibility of intermediate states within ultralow-loss PCM for achieving multistate structural colors through the integration of Sb₂S₃ within the A-DBR structure.

Furthermore, we computed the reflection color bands using eq 3 across various degrees of intermediate crystallinity in Sb₂S₃, as depicted in Figure 3e,f. Figure 3e represents the multistate structural coloring associated with C1, whereas Figure 3f demonstrates the same for C2. The central bandwidths of the reflected color band exhibit a red shift as the degree of crystallinity increases, a phenomenon clearly observed in our experiment as the laser power increases. The calculated central wavelengths for C1 are 630, 650, 675, and 695 nm, correlating to degrees of crystallinity in Sb₂S₃ of 20, 40, 60, and 80%, respectively. On the other hand, at 80% crystallinity, this shifts to 665 nm for the yellow color band (C2 configuration). Therefore, upon reaching 100% crystallinity (cry-Sb₂S₃), the final shift occurs at 735 and 695 nm for the C1 and C2 color bands, respectively. The measured reflectance spectra are broader compared to the calculated reflectance spectra, primarily due to light scattering occurring near the rough interfaces of the A-DBRs. For a further comprehensive grasp of the tuning of the photonic color band, we plotted the central wavelength position of the color band against the degree of crystallinity as shown in Supporting Information Figure S6. Our observations reveal a substantial tuning range of the color band, approximately 110 nm, in both numerical simulations and experimental results.

The reamorphization process of the proposed Sb₂S₃–SiO₂ A-DBR is quite challenging due to the ineffective quenching properties of the SiO₂ layer. The poor thermal conductivity of SiO₂ layers hinders the efficiency of the melt-quenching process during the production of amorphous states from their crystalline state. This difficulty arises due to the challenges in rapidly dissipating heat, affecting the transformation from the crystalline to the amorphous state through the melt-quenching method. To accomplish experimental reverse tuning of the structural color bands, it is essential to substitute SiO₂ with a thermally conductive layer such as Si₃N₄, ZnO, and LiF, among others. On the other hand, although PCM-based color filters offer extensive color tunability over a large scale of visible wavelengths, maintaining color purity in their crystalline phase proves challenging. To tackle this hurdle, we use an in-house-developed iterative neural optimizer⁴⁸ to achieve the high-purity colors both in the amorphous and crystalline phases of Sb₂S₃. The optimizer takes an iterative approach to progressively reduce the target function. The flowchart of the optimization algorithm is shown in Figure 4a, and a comprehensive description of the optimization process is provided in the Supporting Information. The optimizer starts

with some random samples, computing their reflectance spectra, transforming them into CIE color coordinates, and subsequently calculating the corresponding figure of merit (FOM). The figure of merit (FOM) function is defined as

$$\text{FOM} = (x_a - x_0)^2 + (y_a - y_0)^2 + (x_c - x_1)^2 + (y_c - y_1)^2$$

where (x_0, y_0) and (x_1, y_1) are the target color coordinates, and (x_a, y_a) and (x_c, y_c) are the design color coordinates of amorphous and crystalline states, respectively. The optimizer stops when the maximum number of iterations (~ 300) is reached or when the FOM is below a certain threshold (~ 0.001). The FOM curve for the optimization process is shown in Figure 4b. In an optimization aimed to maximize the color contrast, we achieve a blue color for the crystalline DBR with a CIE color coordinate of (0.17, 0.15) and a red color for the amorphous DBR with color coordinates of (0.60, 0.34). Both show high color purity, with their color coordinates located at the boundary of the sRGB (standard red green blue) color standards, as indicated by the dashed line in Figure 4c. These results emphasize the effectiveness of our approach in attaining vibrant and distinctly pure colors in the optimized DBR structure.

In summary, we demonstrated an optically tunable structural coloration using an aperiodic distributed Bragg reflector thin film coating with ultralow-loss Sb₂S₃ PCM as the high refractive index layer. Through the adjustment of layer thicknesses, we achieved highly reflective narrow bandwidths associated with the orange and yellow color bands, exhibiting high color purity (approximately 82–88%) and large color band tunability. Moreover, we demonstrated multistate structural coloring by consciously tuning the spectral band in the forward direction using a laser with variable power density. More significantly, we addressed the limitations associated with current chalcogenide PCM incorporated thin-film coating-based color filters by introducing PCM in the proposed A-DBR structures, offering extensive color tunability, excellent purity, and brightness as well as incident angle and polarization insensitivity. We anticipate that the proposed structural coloring technique will prove to be valuable for advancing next-generation high-purity color display devices and optical data encryptions.

ASSOCIATED CONTENT

Supporting Information

The Supporting Information is available free of charge at <https://pubs.acs.org/doi/10.1021/acs.nanolett.4c00052>.

Sample fabrication and characterization; color purity calculation; optimization method; ellipsometrically measured optical constants; calculated conventional DBR reflection bandwidth; measured CIE color diagram; simulated 2D color map; Raman spectra; central wavelength shiftings, filters comparison table (PDF)

AUTHOR INFORMATION

Corresponding Authors

Ranjan Singh – Division of Physics and Applied Physics, School of Physical and Mathematical Sciences, Nanyang Technological University, Singapore 637371; Centre for Disruptive Photonic Technologies, The Photonic Institute,

Singapore 639798; orcid.org/0000-0001-8068-7428; Email: ranjans@ntu.edu.sg

Jinghua Teng – Institute of Materials Research and Engineering (IMRE), Agency for Science, Technology and Research (A*STAR), Singapore 138634, Republic of Singapore; orcid.org/0000-0001-5331-3092; Email: jhteng@imre.a-star.edu.sg

Authors

Sambhu Jana – Division of Physics and Applied Physics, School of Physical and Mathematical Sciences, Nanyang Technological University, Singapore 637371; Centre for Disruptive Photonic Technologies, The Photonic Institute, Singapore 639798

Kandammathe Valiyaveedu Sreekanth – Institute of Materials Research and Engineering (IMRE), Agency for Science, Technology and Research (A*STAR), Singapore 138634, Republic of Singapore

Omar A. M. Abdelraouf – Institute of Materials Research and Engineering (IMRE), Agency for Science, Technology and Research (A*STAR), Singapore 138634, Republic of Singapore

Ronghui Lin – Institute of Materials Research and Engineering (IMRE), Agency for Science, Technology and Research (A*STAR), Singapore 138634, Republic of Singapore

Hong Liu – Institute of Materials Research and Engineering (IMRE), Agency for Science, Technology and Research (A*STAR), Singapore 138634, Republic of Singapore; orcid.org/0000-0002-3560-9401

Complete contact information is available at:
<https://pubs.acs.org/10.1021/acs.nanolett.4c00052>

Author Contributions

✉ S.J. and K.V.S. contributed equally to this work.

Notes

The authors declare no competing financial interest.

ACKNOWLEDGMENTS

R.S. and S.J. acknowledge the funding support from the Ministry of Education (MOE), Singapore (Grant No. MOET2EP50121-0009). J.T. and K.V.S. acknowledge funding support from the National Research Foundation Singapore under the CRP program (Grant No. NRF-CRP26-2021-0004) and from the A*STAR (Agency for Science, Technology and Research) under the MTC Program (Grant No. M22L1b0110). O.A.M.A. and H.L. acknowledge funding support from an A*STAR AME programmatic grant (Grant No. A18A7b0058). We are thankful to Dr. Giorgio Adamo for helping us to take the SEM image.

REFERENCES

- (1) Gildas, F.; Dan, Y. Review of Nanostructure Color Filters. *J. Nanophotonics* **2019**, *13* (02), 1.
- (2) Xu, T.; Wu, Y.-K.; Luo, X.; Guo, L. J. Plasmonic Nanoresonators for High-Resolution Colour Filtering and Spectral Imaging. *Nat. Commun.* **2010**, *1* (1), 59.
- (3) Song, H. S.; Lee, G. J.; Yoo, D. E.; Kim, Y. J.; Yoo, Y. J.; Lee, D.-W.; Siva, V.; Kang, I.-S.; Song, Y. M. Reflective Color Filter with Precise Control of the Color Coordinate Achieved by Stacking Silicon Nanowire Arrays onto Ultrathin Optical Coatings. *Sci. Rep.* **2019**, *9* (1), 3350.
- (4) Ghobadi, A.; Hajian, H.; Gokbayrak, M.; Butun, B.; Ozbay, E. Bismuth-Based Metamaterials: From Narrowband Reflective Color

Filter to Extremely Broadband near Perfect Absorber. *Nanophotonics* **2019**, *8* (5), 823–832.

(5) Abdelraouf, O. A. M.; Wang, Z.; Liu, H.; Dong, Z.; Wang, Q.; Ye, M.; Wang, X. R.; Wang, Q. J.; Liu, H. Recent Advances in Tunable Metasurfaces: Materials, Design, and Applications. *ACS Nano* **2022**, *16* (9), 13339–13369.

(6) Ko, Y.-H.; Prabhakaran, P.; Choi, S.; Kim, G.-J.; Lee, C.; Lee, K.-S. Environmentally Friendly Quantum-Dot Color Filters for Ultra-High-Definition Liquid Crystal Displays. *Sci. Rep.* **2020**, *10* (1), 15817.

(7) Kang, Y.; Song, Z.; Jiang, X.; Yin, X.; Fang, L.; Gao, J.; Su, Y.; Zhao, F. Quantum Dots for Wide Color Gamut Displays from Photoluminescence to Electroluminescence. *Nanoscale Res. Lett.* **2017**, *12* (1), 154.

(8) Jung, Y.; Jung, H.; Choi, H.; Lee, H. Polarization Selective Color Filter Based on Plasmonic Nanograting Embedded Etalon Structures. *Nano Lett.* **2020**, *20* (9), 6344–6350.

(9) Li, L.; Shi, S.; Escuti, M. J. Improved Saturation and Wide-Viewing Angle Color Filters Based on Multi-Twist Retarders. *Opt. Express* **2021**, *29* (3), 4124.

(10) Ortiz Lizcano, J. C.; Procel, P.; Calcabrini, A.; Yang, G.; Ingenito, A.; Santbergen, R.; Zeman, M.; Isabella, O. Colored Optic Filters on C Si IBC Solar Cells for Building Integrated Photovoltaic Applications. *Prog. Photovoltaics Res. Appl.* **2022**, *30* (4), 401–435.

(11) Jia, P.; Jiang, H.; Sabarinathan, J.; Yang, J. Plasmonic Nanohole Array Sensors Fabricated by Template Transfer with Improved Optical Performance. *Nanotechnology* **2013**, *24* (19), 195501.

(12) Kazuma, E.; Tatsuma, T. Localized Surface Plasmon Resonance Sensors Based on Wavelength-Tunable Spectral Dips. *Nanoscale* **2014**, *6* (4), 2397–2405.

(13) Li, Z.; Butun, S.; Aydin, K. Large-Area, Lithography-Free Super Absorbers and Color Filters at Visible Frequencies Using Ultrathin Metallic Films. *ACS Photonics* **2015**, *2* (2), 183–188.

(14) Abdelraouf, O. A. M.; Wang, X. C.; Goh Ken, C. H.; Lim Nelson, C. B.; Ng, S. K.; Wang, W. De; Renshaw Wang, X.; Wang, Q. J.; Liu, H. All Optical Switching of Structural Color with a Fabry-Pérot Cavity. *Adv. Photonics Res.* **2023**, *4* (11), 2300209.

(15) Dai, P.; Wang, Y.; Hu, Y.; de Groot, C. H.; Muskens, O.; Duan, H.; Huang, R. Accurate Inverse Design of Fabry-Perot-Cavity-Based Color Filters Far beyond SRGB via a Bidirectional Artificial Neural Network. *Photonics Res.* **2021**, *9* (5), B236.

(16) ElKabbash, M.; Letsou, T.; Jalil, S. A.; Hoffman, N.; Zhang, J.; Rutledge, J.; Lininger, A. R.; Fann, C.-H.; Hinczewski, M.; Strangi, G.; Guo, C. Fano-Resonant Ultrathin Film Optical Coatings. *Nat. Nanotechnol.* **2021**, *16* (4), 440–446.

(17) Prabhathan, P.; Sreekanth, K. V.; Teng, J.; Singh, R. Electrically Tunable Steganographic Nano-Optical Coatings. *Nano Lett.* **2023**, *23* (11), 5236–5241.

(18) ElKabbash, M.; Hoffman, N.; Lininger, A. R.; Jalil, S. A.; Letsou, T.; Hinczewski, M.; Strangi, G.; Guo, C. Fano Resonant Optical Coatings Platform for Full Gamut and High Purity Structural Colors. *Nat. Commun.* **2023**, *14* (1), 3960.

(19) Wang, D.; Zhao, L.; Yu, S.; Shen, X.; Wang, J.-J.; Hu, C.; Zhou, W.; Zhang, W. Non-Volatile Tunable Optics by Design: From Chalcogenide Phase-Change Materials to Device Structures. *Mater. Today* **2023**, *68*, 334–355.

(20) Shrestha, V. R.; Lee, S.-S.; Kim, E.-S.; Choi, D.-Y. Non-Iridescent Transmissive Structural Color Filter Featuring Highly Efficient Transmission and High Excitation Purity. *Sci. Rep.* **2014**, *4* (1), 4921.

(21) Sreekanth, K. V.; Medwal, R.; Srivastava, Y. K.; Manjappa, M.; Rawat, R. S.; Singh, R. Dynamic Color Generation with Electrically Tunable Thin Film Optical Coatings. *Nano Lett.* **2021**, *21* (23), 10070–10075.

(22) Sabnis, R. W. Color Filter Technology for Liquid Crystal Displays. *Displays* **1999**, *20* (3), 119–129.

(23) Sun, Y.; Zhang, C.; Yang, Y.; Ma, H.; Sun, Y. Improving the Color Gamut of a Liquid-Crystal Display by Using a Bandpass Filter. *Curr. Opt. Photonics* **2019**, *3* (6), 590–596.

- (24) Sreekanth, K. V.; Jana, S.; ElKabbash, M.; Singh, R.; Teng, J. Phase Change Material-Based Tunable Fano Resonant Optical Coatings and Their Applications. *Nanophotonics* **2024**, DOI: 10.1515/nanoph-2023-0723.
- (25) Huang, Y.-S.; Lee, C.-Y.; Rath, M.; Ferrari, V.; Yu, H.; Woehl, T. J.; Ni, J. H.; Takeuchi, I.; Ríos, C. Tunable Structural Transmissive Color in Fano-Resonant Optical Coatings Employing Phase-Change Materials. *Mater. Today Adv.* **2023**, 18, 100364.
- (26) Sreekanth, K. V.; Perumal, J.; Dinish, U. S.; Prabhathan, P.; Liu, Y.; Singh, R.; Olivo, M.; Teng, J. Tunable Tamm Plasmon Cavity as a Scalable Biosensing Platform for Surface Enhanced Resonance Raman Spectroscopy. *Nat. Commun.* **2023**, 14 (1), 7085.
- (27) Sreekanth, K. V.; Medwal, R.; Das, C. M.; Gupta, M.; Mishra, M.; Yong, K. T.; Rawat, R. S.; Singh, R. Electrically Tunable All-PCM Visible Plasmonics. *Nano Lett.* **2021**, 21 (9), 4044–4050.
- (28) Pitchappa, P.; Kumar, A.; Prakash, S.; Jani, H.; Medwal, R.; Mishra, M.; Rawat, R. S.; Venkatesan, T.; Wang, N.; Singh, R. Volatile Ultrafast Switching at Multilevel Nonvolatile States of Phase Change Material for Active Flexible Terahertz Metadevices. *Adv. Funct. Mater.* **2021**, 31 (17), 2100200.
- (29) Pitchappa, P.; Kumar, A.; Prakash, S.; Jani, H.; Venkatesan, T.; Singh, R. Chalcogenide Phase Change Material for Active Terahertz Photonics. *Adv. Mater.* **2019**, 31 (12), 1808157.
- (30) Abdelraouf, O. A. M.; Anthur, A. P.; Dong, Z.; Liu, H.; Wang, Q.; Krivitsky, L.; Renshaw Wang, X.; Wang, Q. J.; Liu, H. Multistate Tuning of Third Harmonic Generation in Fano-Resonant Hybrid Dielectric Metasurfaces. *Adv. Funct. Mater.* **2021**, 31 (48), 2104627.
- (31) Sreekanth, K. V.; Mahalakshmi, P.; Han, S.; Mani Rajan, M. S.; Choudhury, P. K.; Singh, R. Brewster Mode Enhanced Sensing with Hyperbolic Metamaterial. *Adv. Opt. Mater.* **2019**, 7 (21), 1900680.
- (32) Sreekanth, K. V.; Ouyang, Q.; Sreejith, S.; Zeng, S.; Lishu, W.; Ilker, E.; Dong, W.; ElKabbash, M.; Ting, Y.; Lim, C. T.; Hinczewski, M.; Strangi, G.; Yong, K.; Simpson, R. E.; Singh, R. Phase Change Material Based Low Loss Visible Frequency Hyperbolic Metamaterials for Ultrasensitive Label Free Biosensing. *Adv. Opt. Mater.* **2019**, 7 (12), 1900081.
- (33) Sreekanth, K. V.; Das, C. M.; Medwal, R.; Mishra, M.; Ouyang, Q.; Rawat, R. S.; Yong, K.; Singh, R. Electrically Tunable Singular Phase and Goos-Hänchen Shifts in Phase Change Material Based Thin Film Coatings as Optical Absorbers. *Adv. Mater.* **2021**, 33 (15), 2006926.
- (34) Schubert, M. F.; Xi, J.-Q.; Kim, J. K.; Schubert, E. F. Distributed Bragg Reflector Consisting of High- and Low-Refractive-Index Thin Film Layers Made of the Same Material. *Appl. Phys. Lett.* **2007**, 90 (14), 141115.
- (35) Gao, B.; George, J. P.; Beeckman, J.; Neyts, K. Design, Fabrication and Characterization of a Distributed Bragg Reflector for Reducing the Étendue of a Wavelength Converting System. *Opt. Express* **2020**, 28 (9), 12837.
- (36) Kim, H.; Kaya, M.; Hajimirza, S. Broadband Solar Distributed Bragg Reflector Design Using Numerical Optimization. *Sol. Energy* **2021**, 221, 384–392.
- (37) Sreekanth, K. V.; Prabhathan, P.; Chaturvedi, A.; Lekina, Y.; Han, S.; Zexiang, S.; Tong Teo, E. H.; Teng, J.; Singh, R. Wide Angle Tunable Critical Coupling in Nanophotonic Optical Coatings with Low Loss Phase Change Material. *Small* **2022**, 18 (28), 2202005.
- (38) Chew, L. T.; Zhou, X.; Simpson, R.; Dong, W.; Liu, H.; Valiyaveedu, S. K.; Liu, L.; Cao, T.; Yang, J.; Behera, J.; Mao, L. Chalcogenide Active Photonics. In *Active Photonic Platforms IX*; Subramania, G. S., Foteinopoulou, S., Eds.; SPIE, 2017; p 44. DOI: 10.1117/12.2273732.
- (39) Prabhathan, P.; Sreekanth, K. V.; Teng, J.; Ko, J. H.; Yoo, Y. J.; Jeong, H.-H.; Lee, Y.; Zhang, S.; Cao, T.; Popescu, C.-C.; Mills, B.; Gu, T.; Fang, Z.; Chen, R.; Tong, H.; Wang, Y.; He, Q.; Lu, Y.; Liu, Z.; Yu, H.; Mandal, A.; Cui, Y.; Ansari, A. S.; Bhingardive, V.; Kang, M.; Lai, C. K.; Merklein, M.; Muller, M. J.; Song, Y. M.; Tian, Z.; Hu, J.; Losurdo, M.; Majumdar, A.; Miao, X.; Chen, X.; Gholipour, B.; Richardson, K. A.; Eggleton, B. J.; Wuttig, M.; Singh, R. Roadmap for Phase Change Materials in Photonics and Beyond. *iScience* **2023**, 26 (10), 107946.
- (40) Schanda, J. CIE Chromaticity Diagrams, CIE Purity, CIE Dominant Wavelength. In *Encyclopedia of Color Science and Technology*; Springer International: Cham, Switzerland, 2023; pp 186–190. DOI: 10.1007/978-3-030-89862-5_325.
- (41) Bai, M.; Liu, X.; Sakai, N.; Ebina, Y.; Jia, L.; Tang, D.; Sasaki, T.; Ma, R. General Synthesis of Layered Rare-Earth Hydroxides (RE = Sm, Eu, Gd, Tb, Dy, Ho, Er, Y) and Direct Exfoliation into Monolayer Nanosheets with High Color Purity. *J. Phys. Chem. Lett.* **2021**, 12 (41), 10135–10143.
- (42) Wu, Y.; Nien, Y.; Wang, Y.; Chen, I. Enhancement of Photoluminescence and Color Purity of CaTiO₃:Eu Phosphor by Li Doping. *J. Am. Ceram. Soc.* **2012**, 95 (4), 1360–1366.
- (43) He, Q.; Youngblood, N.; Cheng, Z.; Miao, X.; Bhaskaran, H. Dynamically Tunable Transmissive Color Filters Using Ultra-Thin Phase Change Materials. *Opt. Express* **2020**, 28 (26), 39841.
- (44) Smolovich, A. M.; Kashin, V. V.; Chernov, V. See-through Reflective Optical Elements with Embedded Wavelike Films. *J. Radio Electron.* **2021**. DOI: 10.30898/1684-1719.2021.74.
- (45) Russo, U.; Ielmini, D.; Lacaita, A. L. Analytical Modeling of Chalcogenide Crystallization for PCM Data-Retention Extrapolation. *IEEE Trans. Electron Devices* **2007**, 54 (10), 2769–2777.
- (46) Kumar, A.; Kumar, V.; Romeo, A.; Wiemer, C.; Mariotto, G. Raman Spectroscopy and In Situ XRD Probing of the Thermal Decomposition of Sb₂Se₃ Thin Films. *J. Phys. Chem. C* **2021**, 125 (36), 19858–19865.
- (47) Liu, H.; Dong, W.; Wang, H.; Lu, L.; Ruan, Q.; Tan, Y. S.; Simpson, R. E.; Yang, J. K. W. Rewritable Color Nanoprints in Antimony Trisulfide Films. *Sci. Adv.* **2020**, 6 (51), eabb7171.
- (48) Lin, R.; Valuckas, V.; Do, T. T. H.; Nemati, A.; Kuznetsov, A. I.; Teng, J.; Ha, S. T. Schrödinger's Red Beyond 65,000 Pixel Per Inch by Multipolar Interaction in Freeform Meta Atom through Efficient Neural Optimizer. *Adv. Sci.* **2023**, 2303929.